# Saturation of Gyrokinetic Turbulence through Damped Eigenmodes

D. R. Hatch,[1] P. W. Terry,[1] F. Jenko,[2] F. Merz,[2] and W. M. Nevins[3]
[1]*University of Wisconsin–Madison, Madison, Wisconsin 53706, USA*
[2]*Max-Planck-Institut für Plasmaphysik, EURATOM Association, 85748 Garching, Germany*
[3]*Lawrence Livermore National Laboratory, Livermore, California 94550, USA*
(Received 23 June 2010; revised manuscript received 25 January 2011; published 16 March 2011)

In the context of toroidal gyrokinetic simulations, it is shown that a hierarchy of damped modes is excited in the nonlinear turbulent state. These modes exist at the same spatial scales as the unstable eigenmodes that drive the turbulence. The larger amplitude subdominant modes are weakly damped and exhibit smooth, large-scale structure in velocity space and in the direction parallel to the magnetic field. Modes with increasingly fine-scale structure are excited to decreasing amplitudes. In aggregate, damped modes define a potent energy sink. This leads to an overlap of the spatial scales of energy injection and peak dissipation, a feature that is in contrast with more traditional turbulent systems.

DOI: 10.1103/PhysRevLett.106.115003 PACS numbers: 52.30.Gz, 52.35.Qz, 52.35.Ra, 52.65.Tt

In high Reynolds number fluid turbulence, as modeled by the Navier-Stokes equation, energy is injected at large scales and conservatively transferred by nonlinear interactions through a broad inertial range to a dissipation range at small scales [1]. Saturation is achieved when the rate of energy injection at large scales is balanced by the rate of energy dissipation at small scales. Saturation theories for plasma microturbulence typically involve variations on this theme. Indeed, such an energy cascade occurs in both physical space and velocity space for small-scale ($k_\perp \rho_i \gg 1$, where $k_\perp$ is the wave number perpendicular to the magnetic field and $\rho_i$ is the ion gyroradius), homogeneous, two-dimensional, decaying plasma turbulence [2]. For toroidal fusion plasmas, conventional wisdom also holds that dissipation occurs largely at small spatial scales. This is consistent, for example, with the notion that zonal flows suppress turbulence by shearing, an inertial process that enhances transfer to small scales [3]. In this work, we show that for ion temperature gradient (ITG) driven turbulence in toroidal fusion plasmas as modeled by the gyrokinetic equations, dissipation occurs at *all* spatial scales, peaking at the large scales including those where the instability drives the turbulence. This is made possible by the nonlinear excitation of damped modes at the same spatial scales as the unstable eigenmodes that drive the turbulence. This excitation of a large number of damped modes makes plasma microturbulence much different from hydrodynamic turbulence in a way not fully appreciated before.

The instabilities that drive plasma microturbulence are mathematically defined as eigenmodes of a linear operator. In almost all microturbulence models, the unstable eigenmodes are accompanied by stable eigenmodes which have typically been neglected in analyses of turbulent dynamics. Recent work has shown that damped eigenmodes are critical in understanding saturation and transport in fluid models of plasma microturbulence [4]. Initial efforts have been made to examine the effect in gyrokinetics [5]. In this work, the explicit role of damped modes in gyrokinetic simulations is examined for the first time.

The gyrokinetic model solves for the gyrocenter distribution function $g$, representing the perturbed distribution of guiding centers (deviation from Maxwellian). It is a function of six variables: three spatial coordinates (the radial direction $x$, the mostly poloidal binormal direction $y$, and the direction parallel to the magnetic field, $z$), two velocity coordinates (represented here by parallel velocity $v_\parallel$ and magnetic moment $\mu$), and time. The adiabatic electron assumption reduces the problem to a single ion distribution function. We employ the flux-tube representation [6] allowing a Fourier decomposition in $x$ and $y$. The resulting wave numbers ($k_x$ and $k_y$), which we will call wave vectors in this Letter, are coupled through the nonlinearity of the gyrokinetic equation. At issue is the dependence of energy dissipation on these perpendicular scales.

When studying linear stability in plasma microturbulence, one selects a wave vector and solves for the eigenvalues and eigenvectors of a linear differential operator. In gyrokinetics, linear analysis is frequently limited to an initial value simulation; when there is an instability at this wave vector, the eigenmode with the largest growth rate grows exponentially and eventually dominates the solution. The resulting solution for the distribution function can be expressed as $g_{k_x,k_y}(z, v_\parallel, \mu, t) = f(z, v_\parallel, \mu)h(t)$, where $f$ defines the mode structure and $h$ defines the time dependence in the form of $e^{-i(\omega+i\gamma)t}$. For the parameters used in this study, the ITG instability is the only instability in the system, and at each wave vector there is at most one unstable eigenmode. The region of instability is at large scales, approximately $k_x\rho_i \approx (-1/2, 1/2)$ and $k_y\rho_i \approx (\pm k_{y_{\min}}\rho_i, \pm 1/2)$. Outside of this region, at smaller spatial scales, all linear eigenmodes are stable, which contributes to the conventional wisdom that dissipation occurs predominantly at small scales. However, in the region of instability, despite the presence of unstable eigenmodes,

 

there also exist stable eigenmodes that can provide a means of energy dissipation provided they are driven to finite amplitude by nonlinear interactions. For each wave vector, numerical discretization allows for $N = n_z \times n_{v_\parallel} \times n_\mu$ degrees of freedom, where the $n$'s denote the number of grid points in each coordinate. The unstable eigenmode defines only one of these degrees of freedom; the remaining degrees of freedom provide an energy sink at large spatial scales.

We seek to characterize the nonlinear state by decomposing the gyrokinetic distribution function for selected wave vectors ($k_x$ and $k_y$) as a superposition of modes:

$$g_{k_x,k_y}(z, v_\parallel, \mu, t) = \sum_n f^{(n)}_{k_x,k_y}(z, v_\parallel, \mu) h^{(n)}_{k_x,k_y}(t). \quad (1)$$

The structure $f^{(1)}(z, v_\parallel, \mu)$ corresponds to the unstable eigenmode, but its time amplitude $h^{(1)}(t)$, rather than exhibiting its linear behavior $e^{-i(\omega+i\gamma)t}$, fluctuates as determined by a balance between the linear drive and the stabilizing influence of nonlinear interactions. The other modes are also defined by fixed mode structures $f^{(n)}(z, v_\parallel, \mu)$ and fluctuate according to their respective time amplitudes $h^{(n)}(t)$ in such a way that a superposition of all the modes exactly reproduces the total distribution function at each moment in time. In contrast with the unstable mode, the time amplitudes $h^{(n)}(t)$ of damped modes fluctuate according to a balance between nonlinear drive and linear damping, the latter of which dissipates energy from the system, thereby facilitating saturation of the turbulence. This decomposition is constructed by performing a proper orthogonal decomposition (POD) [7,8] on data from a standard nonlinear gyrokinetic simulation. This provides a means to examine separately the contribution of individual modes, stable or unstable, to the saturation of the turbulence.

To study the role of damped modes in saturation, we track energy injected into or removed from the turbulence by using diagnostics related to the conserved (in the absence of drive and dissipation) energylike quantity [9] $E = \int dv_\parallel d\mu dz B_0 \pi n_0 T_0 |g|^2/F_0 + \int dz D(k_\perp, z)|\phi|^2$, where $B_0$ is the equilibrium magnetic field, $\phi$ is the electrostatic potential, $n_0$ and $T_0$ are the background density and temperature, respectively, and $D$ is a function of $z$ and the perpendicular wave numbers. The energy evolves according to

$$\left.\frac{\partial E_k}{\partial t}\right|_{\text{N.C.}} = Q_k + C_k, \quad (2)$$

where $Q = \int dv_\parallel d\mu dz \pi n_0 T_0 B_0 / L_T (v_\parallel^2 + \mu B_0) g^* i k_y \bar{\phi}$ is a term proportional to the heat flux and includes the turbulent drive ($\bar{\phi}$ is the gyro-averaged potential, and $L_T$ is the temperature gradient scale length), $C$ represents collisional dissipation, and, in a simulation, whatever artificial dissipation (e.g., hyperdiffusive terms) is included in the code. The subscript N.C. indicates that this equation describes only the nonconservative energy evolution, i.e., processes that inject or dissipate net energy from the fluctuations (as opposed to processes like the $E \times B$ nonlinearity that move energy from one scale to another in a conservative fashion).

The GENE code [10] is used to simulate ITG driven turbulence defined by the cyclone base case parameters [11] of safety factor $q = 1.4$, magnetic shear $\hat{s} = 0.8$, inverse aspect ratio $\epsilon = r/R = 0.18$, equilibrium ratios of density and temperature $n_i/n_e = T_i/T_e = 1.0$, and background gradients $R/L_T = 6.9$ and $R/L_n = 2.2$, where $R$ is the major radius. The perpendicular box size is $(L_x, L_y) = (126\rho_i, 126\rho_i)$, and the number of grid points is $32 \times 48 \times 8$ for the $(z, v_\parallel, \mu)$ coordinates, respectively. The perpendicular spatial resolution consists of 128 grid points in the $x$ direction giving $k_{x,\max}\rho_i = 3.12$ and 64 $k_y$ Fourier modes for $k_{y,\max}\rho_i = 3.15$. We deviate from the cyclone base case by using a linearized Landau-Boltzmann collision operator rather than exclusively artificial dissipation. The collision frequency is $\nu(R/v_T) = 3.0 \times 10^{-3}$, which is much less than the dynamic time scales of the system [e.g., the most unstable mode at $k_y\rho_i = 0.3$ has a growth rate $\gamma(R/v_T) = 0.267$ and frequency $\omega(R/v_T) = 0.783$ so that $\nu/\omega \sim 10^{-2}$]. In these runs, $C_k$ consists mostly of collisional dissipation but also includes contributions from fourth-order hyperdiffusive dissipation in the $z$ and $v_\parallel$ coordinates.

To illustrate the spatial scale dependence of the energy balance, we first consider separately the drive term $Q_k$ and the dissipation term $C_k$ in Eq. (2). Figure 1 shows $Q_k$ and $C_k$ from the saturated state of a simulation, averaged over the parallel coordinate and time. In Fig. 1(a), $k_x$ dependence is shown and $k_y$ is summed; in Fig. 1(b), $k_y$ dependence is shown and $k_x$ is summed. There is a significant amount of dissipation at all scales, including $k_y = 0.0$ and high $k_\perp$. However, the largest range of peak dissipation corresponds with the same scales where the energy drive peaks. As described in detail below, the drive $Q_k$ is

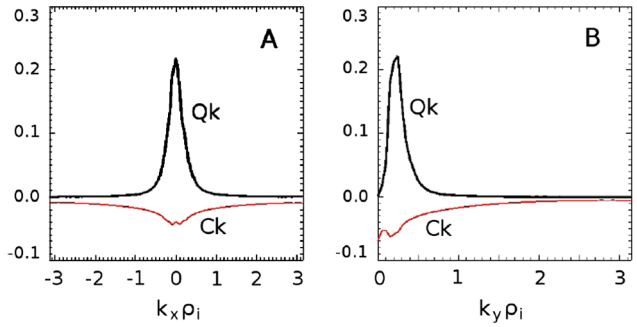


FIG. 1 (color online). Energy drive $Q_k$ and dissipation $C_k$ time averaged over the nonlinear state and averaged over the $z$ direction, as a function of (a) $k_x$ summed over $k_y$ and (b) $k_y$ summed over $k_x$.

dominated by the unstable modes, while the dissipation $C_k$ is dominated by the stable modes. Contrast this with the corresponding scenario in high Reynolds number Navier-Stokes turbulence for which the drive is localized at large scales, the dissipation is localized at small scales, and there is a broad inertial range of intermediate scales with neither drive nor dissipation.

The observed $k$ dependence of the dissipation is due to the excitation of a hierarchy of damped modes in the nonlinear state. POD analysis elegantly characterizes this hierarchy of modes. POD uses the singular value decomposition [12] of a matrix to create an optimal orthonormal basis for fluctuation data. In this application, each column of the input matrix consists of a time slice (at every 50 time steps) of the nonlinearly evolved gyrokinetic distribution function for a selected wave vector. The nonspectral coordinates $(z, v_\parallel, \mu)$ are unraveled to one dimension, e.g., as the data would be stored in computer memory. The singular values $s_n$ define the amplitudes of the $n$th modes. The left singular vectors are the POD modes—basis vectors that are orthonormal with regard to the scalar product $\oint f^{(n)^*} f^{(m)} J(z) dz dv_\parallel d\mu$, where $J(z)$ is a Jacobian [these correspond to $f^{(n)}(z, v_\parallel, \mu)$ in Eq. (1)]. The right singular vectors are time traces of the amplitudes of the corresponding POD modes [these, multiplied by the singular values, correspond to $h^{(n)}(t)$ in Eq. (1)].

It is observed that, for wave vectors with a strongly unstable eigenmode, the $n = 1$ POD mode is very similar to the unstable linear eigenmode, they exhibit nearly identical mode structures, and the scalar product between the two is $\sim$0.9. As a result, for much of this study we will conceptually equate the $n = 1$ POD mode with the corresponding unstable linear eigenmode.

In order to elucidate the energy drive and dissipation processes in the instability range, we will examine in detail the POD analysis of the wave vector of peak transport: $k_y\rho_i = 0.2$ and $k_x\rho_i = 0.0$. These results are representative of other important energy-containing wave vectors in the spectrum. The POD singular values decay rapidly in mode number $n$ up to $n \sim 100$. At that point and beyond, the spectrum exhibits exponential decay as seen in Fig. 2(a). Further insight can be gained by calculating $Q_k$ and $C_k$ for each mode $f^{(n)}(z, v_\parallel, \mu)$. In these calculations $Q_k + C_k$ can, in a sense, be conceptualized as growth (or damping) rates since the modes are normalized and contain no amplitude dependence. The mode-by-mode values of $C_k$ are all negative and increase strongly in amplitude with mode number, as seen in Fig. 2(c). As expected, the first POD mode produces a large positive value of $Q_k$. The remaining modes are associated with amplitudes of $Q_k$ which decrease with mode number and have seemingly random signs; i.e., their $\phi^*T$ phase angles are randomly distributed around zero. This is shown in Fig. 2(b). These results differ from fluid models, where the damped eigenmodes are stable due to a large and systematic effect on

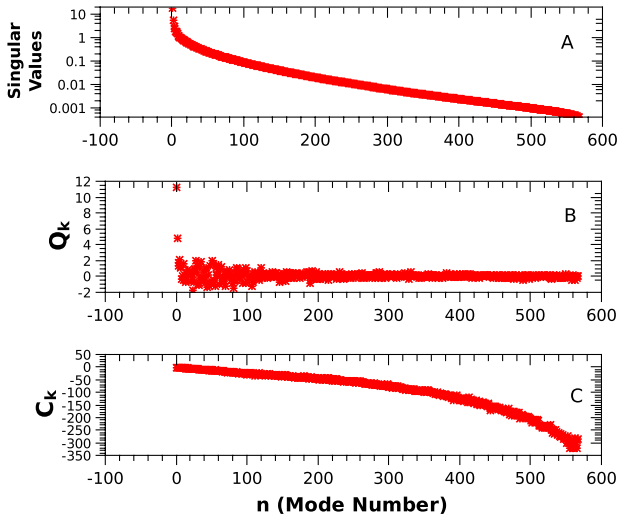


FIG. 2 (color online). The spectrum of singular values (a), energy drive $Q_k$ for each normalized POD mode (b), and dissipation $C_k$ for each normalized mode (c). For $k_y\rho_i = 0.2$, $k_x\rho_i = 0.0$.

cross correlations like $\phi^*T$ [4] (in contrast with the modes described here, which are damped due to collisional dissipation).

The contribution of the $n > 1$ modes to the energy balance can be separated from that of the unstable $(n = 1)$ mode by decomposing the distribution function as $g = f^{(1)}h^{(1)} + f^{(\mathrm{res})}h^{(\mathrm{res})}$, where the residual distribution function $f^{(\mathrm{res})}h^{(\mathrm{res})}$ is the sum of the $n > 1$ POD modes and represents all fluctuations not associated with the unstable mode. It is found that the energy drive $Q_k$ is dominated by the unstable mode, whereas the dissipation $C_k$ is dominated by the residual distribution function. This can be seen by examining a selection of wave vectors in the region of instability centered around the peak of the spectrum $(k_x\rho_i = 0.0,\ k_y\rho_i = [0.05, 0.2, 0.3, 0.4]$, and $k_y\rho_i = 0.2$, $k_x\rho_i = [0.1, 0.2, 0.4])$. For the sum of these wave vectors, the residual drive $Q_k(f^{(\mathrm{res})}) \int |h^{(\mathrm{res})}(t)|^2 dt$ accounts for only 7% of the total energy drive, but the residual dissipation $C_k(f^{(\mathrm{res})}) \int |h^{(\mathrm{res})}(t)|^2 dt$ accounts for 63% of the total dissipation. Both the dissipation associated with the $n = 1$ mode and the residual dissipation peak at $k_y\rho_i = 0.2$, $k_x\rho_i = 0.0$ and decrease as $k_\perp$ increases. In summary, unstable eigenmodes (collectively represented here by $f^{(1)}_{k_x,k_y}$) drive the turbulence. Nonlinear interactions excite linearly damped modes (represented here by $f^{(res)}_{k_x,k_y}$) at the same perpendicular scales ($k_x$ and $k_y$) as the driving instability. The excitation of these modes causes the dissipation to peak at large perpendicular scales. The calculation in this paragraph, in conjunction with Fig. 1, establishes the main claim of this Letter; Fig. 1 shows that the scale range of energy drive and dissipation overlap, and this calculation demonstrates that, in this same scale range, the dissipation is dominated by modes other than the unstable mode.

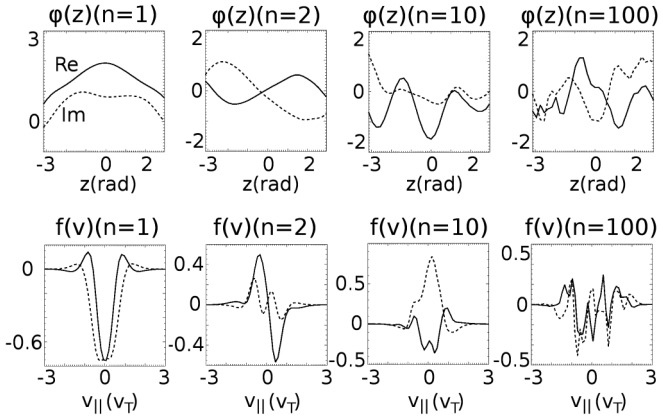


FIG. 3. Mode structures for a selection of POD modes at the peak of the nonlinear spectrum, $k_y\rho_i = 0.2$, $k_x\rho_i = 0.0$. The mode structures of the electrostatic potential are shown in the top row for modes 1, 2, 10, and 100, and the $v_\parallel$ dependence is shown in the bottom row for the same POD modes at $\mu = 0.18$ and $z = 0$. Fine-scale structure develops in both coordinates as $n$ increases.

In order to characterize the POD modes and describe their role in the energetics, we show in Fig. 3 mode structures for selected POD modes for the wave vector of peak transport: $k_y\rho_i = 0.2$, $k_x\rho_i = 0.0$. In the top row of Fig. 3, the parallel mode structures for the electrostatic potential are plotted (for POD modes 1, 2, 10, and 100), and in the bottom row the $v_\parallel$ dependence is shown (for the same POD modes at $\mu = 0.18$ and $z = 0$). As mentioned above, the $n = 1$ POD modes are very similar to the unstable linear eigenmodes. The second most important structure, the $n = 2$ POD mode, is also very similar to a linear eigenmode. This linear eigenmode is the most weakly damped stable mode, having a damping rate an order of magnitude smaller than the growth rate of the ITG mode. Figure 3 also demonstrates the fine-scale structure that develops in the $z$ and $v_\parallel$ coordinates. The scale lengths in the $z$ and $v_\parallel$ coordinates both decrease as $n$ increases. As a result, these modes become increasingly dissipative due to the higher-order derivatives in the dissipation operators. The development of fine-scale structure in $v_\parallel$ is consistent with aspects of linear phase mixing [13]. There must also be a nonlinear excitation mechanism involved in the process since the linear system produces only the unstable mode (all other eigenmodes decay exponentially). An effort to better understand this phenomenon will be an aspect of future work.

The results presented in this Letter do not contradict the numerically observed power law $k_\perp$ spectra reported in the literature [2,14,15]. From a dissipation range analysis [16] a spectrum goes as $k^{-\alpha}\exp[c(k/k_d)^{-\beta}]$, where $k_d$ is the wave number at which damping and nonlinear decorrelation rates are equal, $c$ is a positive constant, and $0 < \beta < 2/3$, provided the damping increases with wave number $k$ more slowly than the nonlinear decorrelation rate. This condition appears to be satisfied for the data presented here. This spectrum transitions to a regime dominated by the power law behavior for high $k$. An analysis of high-$k_\perp$ spectra for simulations very similar to those presented in this Letter is provided in Ref. [15], where power law spectra agree quite well with those described in Ref. [2].

The following is a plausible saturation scenario: Through collisional dissipation, damped modes dissipate a significant portion of the injected energy at the same spatial scales as the instability operates ($k_\perp\rho_i \lesssim 1$). This is accompanied by a spatial cascade carrying energy to smaller perpendicular scales ($k_\perp\rho_i > 1$). At these smaller scales, the remaining dissipation occurs and processes such as nonlinear perpendicular phase mixing dominate.

In summary, we have shown that, in ITG driven turbulence modeled by the gyrokinetic equations, dissipation occurs at all scales, peaking in the wave number range of the instability drive. The dissipation is associated with a very large number of damped eigenmodes excited to finite amplitude by nonlinearity.

This research was performed under the U.S. Department of Energy Contract No. DE-AC05-060R23100 between the U.S. Department of Energy and Oak Ridge Associated Universities.

[1] A. N. Kolmogorov, Dokl. Akad. Nauk SSSR **30**, 299 (1941).
[2] T. Tatsuno *et al.*, Phys. Rev. Lett. **103**, 015003 (2009).
[3] P. H. Diamond *et al.*, Plasma Phys. Controlled Fusion **47**, R35 (2005).
[4] See, e.g., P. W. Terry, D. A. Baver, and S. Gupta, Phys. Plasmas **13**, 022307 (2006).
[5] D. R. Hatch *et al.*, Phys. Plasmas **16**, 022311 (2009).
[6] M. A. Beer, S. C. Cowley, and G. W. Hammett, Phys. Plasmas **2**, 2687 (1995).
[7] G. Berkooz, P. Holmes, and J. L. Lumley, Annu. Rev. Fluid Mech. **25**, 539 (1993).
[8] S. Futatani, S. Benkadda, and D. del-Castillo-Negrete, Phys. Plasmas **16**, 042506 (2009).
[9] T.-H. Watanabe and H. Sugama, Nucl. Fusion **46**, 24 (2006).
[10] F. Jenko *et al.*, Phys. Plasmas **7**, 1904 (2000).
[11] A. M. Dimits *et al.*, Phys. Plasmas **7**, 969 (2000).
[12] G. H. Golub and C. F. Van Loan, *Matrix Computations* (The Johns Hopkins University Press, Baltimore, 1989), 2nd ed.
[13] G. W. Hammett, W. Dorland, and F. W. Perkins, Phys. Fluids B **4**, 2052 (1992).
[14] T. Görler and F. Jenko, Phys. Plasmas **15**, 102508 (2008).
[15] A. Bañón Navarro *et al.*, Phys. Rev. Lett. **106**, 055001 (2011).
[16] P. W. Terry and V. Tangri, Phys. Plasmas **16**, 082305 (2009).